SOLITARY WAVE INTERACTION WITH POROUS BREAKWATERS

By Patrick J. Lynett,[1] Associate Member, ASCE, Philip L.-F. Liu,[2] Fellow, ASCE, Inigo J. Losada,[3] Associate Member, ASCE, and Cesar Vidal[4]

ABSTRACT: This paper presents a numerical model for long-wave interaction with vertically walled porous structures. Based on depth-integrated equations of motion, the model is suitable for weakly nonlinear, weakly dispersive transient waves propagating in both variable-depth open water and porous regions. Comparisons with experimental data for problems with one horizontal dimension show that a single choice of empirical parameters for hydraulic conductivity gives accurate numerical predictions for various sizes of rocks used in the construction of porous breakwaters. A rigorous experimental comparison of a porous breakwater gap shows that the numerical model is excellent in predicting the waveform and phase of the transformed wave. In this paper attention is focused on the reflection, transmission, and diffraction of solitary waves by a porous breakwater.

INTRODUCTION

The interaction of nonlinear, shallow water waves with porous breakwaters is an important subject in coastal planning and design. Many researchers have studied reflection and transmission characteristics of porous rubble-mound breakwaters, but few have examined the diffraction associated with detached porous breakwaters. In most existing works, the incident waves are assumed to be linear and periodic. Sollitt and Cross (1972) and Madsen (1974) introduced linear wave models in which inertia and resistance forces due to a rectangular porous structure were included. Various additions and extensions have been made to these models (Madsen and White 1975; Sulisz 1985). More recently, complex numerical models have given researchers the ability to accurately model virtually any type of coastal setup (van Gent 1995; Liu et al. 1999). These models include only one horizontal dimension and therefore cannot currently be extended to diffraction analysis.

Diffraction of waves by a solid breakwater has received a considerable amount of attention. The earliest work is the adaptation of light diffraction to water waves (Penny and Price 1952), which is still used as a benchmark comparison for research [e.g., Yu and Togashi (1996)] and can be found in most design manuals [e.g., Coastal Engineering Research Center (CERC) (1984)]. Additional analytical diffraction theories have since been developed (Goda et al. 1978; Liu 1984; Dalrymple and Martin 1990), but all require linear waves and constant water depth. Numerical work by Wang (1993) extended solid breakwater diffraction to weakly nonlinear long waves, using Wu's generalized Boussinesq model (Wu 1981). This model was applied to arbitrarily incident waves interacting with a thin breakwater in a constant depth region but could be altered to use a variable-width breakwater in varying water depth. Wang (1993) compared his numerical solution to Liu's linear model and experimental data (Liu 1984), showing that the weakly nonlinear model better predicted the arrival time of the diffracting wave, although both models predicted wave height well.

Diffraction of waves by a porous breakwater, however, has received very little attention. Yu (1995) developed a porous breakwater diffraction model based on the linear potential wave theory. This model was extended to waves of arbitrary incidence (Yu and Togashi 1996; McIver 1999) but requires that the breakwater be thin compared to the incident wave length. Additionally, there are no rigorous experimental studies of porous breakwater diffraction.

This paper presents a numerical model describing the interaction of a weakly nonlinear and weakly dispersive wave train with a porous breakwater as it propagates over variable water depth. The model consists of two components. In the open water region, the model employs the generalized Boussinesq equations presented originally by Wu (1981). Inside the porous breakwater, the model is based on the Boussinesq-type equations derived by Liu and Wen (1997). A high-order predictor-corrector finite-difference scheme is developed to couple two sets of governing equations. Because drag coefficients in the porous media flow need to be determined, laboratory experiments for both 1D solitary wave reflection and transmission and 2D solitary wave diffraction are performed. Very good agreement between the experimental data and numerical results is obtained. This paper focuses on solitary wave diffraction, primarily due to the experimental difficulty in studying periodic wave diffraction. However, with this rigorous soliton diffraction validation and a future validation of 1D breakwater interaction with periodic waves, the model would be proven accurate for periodic wave diffraction as well.

THEORY

In the open-water region, the generalized Boussinesq two-equation model (Wu 1981) is used to describe wave motion. This model has shown to be both stable and accurate in the numerical prediction of solitary and cnoidal wave transformation in the horizontal plane (Wang 1993; Jiang et al. 1996). The equations are in terms of the free-surface displacement ζ and depth-averaged velocity potential ϕ and include weakly nonlinear and weakly dispersive effects. They are given, in dimensional form

$$\frac{\partial \zeta}{\partial t} + \nabla \cdot [(\zeta + h)\nabla \phi] = 0 \tag{1}$$

$$\frac{\partial \phi}{\partial t} + \frac{1}{2}(\nabla \phi)^2 + g\zeta - \frac{h}{2}\frac{\partial}{\partial t}\nabla \cdot (h\nabla \phi) + \frac{h^2}{6}\frac{\partial}{\partial t}\nabla^2 \phi = 0 \tag{2}$$

where h = local water depth; g = gravity; and $\nabla = (\partial/\partial x, \partial/\partial y)$, the horizontal gradient. Depth-averaged velocity $\mathbf{u}$ can be directly calculated with the knowledge of ϕ

$$\mathbf{u} = \nabla \phi \tag{3}$$

Note that the above equations can accommodate changing

[1]Grad. Res. Asst., School of Civ. and Envir. Engrg., Cornell Univ., Ithaca, NY 14853.
[2]Prof., School of Civ. and Envir. Engrg., Cornell Univ., Ithaca, NY.
[3]Prof., Oc. and Coast. Res. Group, Universidad de Cantabria, Santander, Spain.
[4]Assoc. Prof., Oc. and Coast. Res. Group, Universidad de Cantabria, Santander, Spain.

Note. Discussion open until May 1, 2001. To extend the closing date one month, a written request must be filed with the ASCE Manager of Journals. The manuscript for this paper was submitted for review and possible publication on October 18, 1999. This paper is part of the ***Journal of Waterway, Port, Coastal, and Ocean Engineering***, Vol. 126, No. 6, November/December, 2000. ©ASCE, ISSN 0733-950X/00/0006-0314–0322/$8.00 + $.50 per page. Paper No. 22093.

water depth, $h(x, y)$, and are valid only for weakly nonlinear and dispersive waves, i.e.

$$O\left(\frac{a}{h}\right) = O\left[\left(\frac{h}{\lambda}\right)^2\right] << 1 \tag{4}$$

where a represents the wave amplitude; and λ represents the characteristic horizontal length scale of the wave motion.

In the porous region, a set of Boussinesq-type equations is employed. Liu and Wen (1997) derived a set of equations describing long-wave propagation in a porous medium, given in a fully nonlinear form, evaluated on a prescribed horizontal surface. To be consistent with the generalized Boussinesq model for the free surface, Liu and Wen's equations are truncated to include only weakly nonlinear effects and then are averaged over the entire water depth. Denoting ψ as the depth-averaged piezometric head, K as the hydraulic conductivity, n_e as the effective porosity of the porous material, and h as the local water depth, the governing equations for ζ and ψ can be expressed

$$\frac{\partial \zeta}{\partial t} - \frac{K}{n_e}\nabla\cdot[(\zeta + h)\nabla\zeta] - \frac{h^2}{3}\frac{\partial}{\partial t}\nabla^2\zeta = 0 \tag{5}$$

$$\psi = \zeta - \frac{h^2}{3}\nabla^2\zeta \tag{6}$$

Depth-averaged velocity is given

$$\mathbf{u} = -K\nabla\psi \tag{7}$$

In the porous region, the wave characteristics are subject to the restriction indicated by (4). Although the original set of porous flow equations given by Liu and Wen (1997) can accommodate changing depth, in this analysis the reasonable assumption of constant depth in the porous region is made, thus simplifying the porous region equations. It would be straightforward to modify the governing equations so as to include variable depth effects inside the porous region. Additionally, it is required that the porous medium be homogeneous and isotropic; therefore, K must be constant in space.

NUMERICAL MODEL

In this paper, a finite-difference model is presented that couples the Boussinesq equations for water waves with those for free-surface flows within a porous medium. The model structure is similar to that of Wei and Kirby (1995). A high-order predictor-corrector scheme is utilized employing a third-order-in-time explicit Adams-Bashforth predictor step and a fourth-order-in-time Adams-Moulton implicit corrector step (Press et al. 1989). The implicit corrector step must be iterated until a convergence criterion is satisfied. All spatial derivatives are differenced to fourth-order accuracy, yielding a model that is numerically accurate to Δx^4, ϕy^4 in space, and Δt^4 in time.

In the porous region, a set of predictor-corrector equations is required to determine ζ, and ψ is then calculated directly from (6). A grouping of the time derivatives in (5) is done to simplify the predictor-corrector equations. The grouping is given

$$Z = \zeta - \frac{h^2}{3}(\zeta_{xx} + \zeta_{yy}) \tag{8}$$

where subscripts denote partial derivatives. Note that $\psi = Z$, so no additional calculation is needed to determine ψ. The predictor equation used to find ζ in the porous region becomes

$$Z_{i,j}^{n+1} = Z_{i,j}^{n} - \frac{\Delta t}{12}(23P_{i,j}^{n} - 16P_{i,j}^{n-1} + 5P_{i,j}^{n-2}) \tag{9}$$

where

$$P = -\frac{K}{n_e}[\{(\zeta + h)\zeta_x\}_x + \{(\zeta + h)\zeta_y\}_y] \tag{10}$$

All terms are evaluated at the local grid point (i, j), and n represents the current time step when values of ζ, ϕ, and ψ are known. The fourth-order implicit corrector expression for ζ in the porous region is

$$Z_{i,j}^{n+1} = Z_{i,j}^{n} - \frac{\Delta t}{24}(9P_{i,j}^{n+1} + 19P_{i,j}^{n} - 5P_{i,j}^{n-1} + P_{i,j}^{n-2}) \tag{11}$$

In the open-water region, predictor-corrector equations for both ζ and ϕ are required. The time derivatives in (2) are grouped in a manner similar to the grouping given in (8), i.e.

$$\Theta = \phi - \frac{h^2}{3}(\phi_{xx} + \phi_{yy}) - \frac{h}{2}(h_x\phi_x + h_y\phi_y) \tag{12}$$

The predictor equations have the same basic form as those for the porous region

$$\zeta_{i,j}^{n+1} = \zeta_{i,j}^{n} - \frac{\Delta t}{12}(23E_{i,j}^{n} - 16E_{i,j}^{n-1} + 5E_{i,j}^{n-2}) \tag{13}$$

$$\Theta_{i,j}^{n+1} = \Theta_{i,j}^{n} - \frac{\Delta t}{12}(23F_{i,j}^{n} - 16F_{i,j}^{n-1} + 5F_{i,j}^{n-2}) \tag{14}$$

where

$$E = [(\zeta + h)\phi_x]_x + [(\zeta + h)\phi_y]_y \tag{15}$$

$$F = \frac{1}{2}[(\phi_x)^2 + (\phi_y)^2] + g\zeta \tag{16}$$

The corrector equations are

$$\zeta_{i,j}^{n+1} = \zeta_{i,j}^{n} - \frac{\Delta t}{24}(9E_{i,j}^{n+1} + 19E_{i,j}^{n} - 5E_{i,j}^{n-1} + E_{i,j}^{n-2}) \tag{17}$$

$$\Theta_{i,j}^{n+1} = \Theta_{i,j}^{n} - \frac{\Delta t}{24}(9F_{i,j}^{n+1} + 19F_{i,j}^{n} - 5F_{i,j}^{n-1} + F_{i,j}^{n-2}) \tag{18}$$

The system is solved by first evaluating the predictor equations, then solving for ζ in the porous region and ϕ from (8) and (12). For the 2D problem, neither (8) nor (12) yields a diagonal matrix after finite differencing and an iterative Gauss-Seidel method is used to solve the matrix system. If a 1D problem is examined, however, the matrix is diagonal, with a bandwidth of five (due to five-point finite differencing), and an efficient LU decomposition can be utilized. At this point in the numerical system, one has predictors for ζ, ϕ, and ψ. Next, the corrector expressions are evaluated, and ζ in the porous region and ϕ are calculated. The relative errors in each of the physical variables is found to determine if the implicit correctors need to be reiterated. This relative error is given

$$\frac{w^{n+1} - w_*^{n+1}}{w^{n+1}} \tag{19}$$

where w represents ζ, ϕ, and ψ; and w_* = previous iteration's value. The correctors are recalculated until all errors are $<10^{-4}$. Note that inevitably there will be locations in the numerical domain where values of the physical variables are close to zero and applying the above error calculation to these points may lead to unnecessary iterations in the corrector loop. Thus it is required that $|\zeta/a|$, $|\phi/(h\sqrt{ga})|$, and $|\psi/a| > 10^{-4}$ for the corresponding error calculation to proceed.

The grid size is determined such that there are 30 grid points per wavelength. However, it also was found that there should be at least eight grid points inside the porous region in either the x- or y-direction to make certain that the governing equations are actually applied at a sufficient number of locations. For the Boussinesq equations, linear stability analysis shows

that $\Delta t < (\Delta x/2c)$, where c is the wave celerity. For the porous equations, this relationship does not yield a stable numerical model and $\Delta t < (\Delta x/10c)$ gives stable results in all trials.

Along the interface between the open-water and porous regions, it is necessary to match both free-surface displacement and velocity. Additionally, it is required that the spatial derivative of the free surface is continuous across the interface. The interface boundary conditions are

$$\zeta|_+ = \zeta|_-; \quad \mathbf{u}|_+ = \mathbf{u}|_- \tag{20}$$

$$\mathbf{n}\cdot\nabla\zeta|_+ = \mathbf{n}\cdot\nabla\zeta|_- \tag{21}$$

where the sign denotes opposite sides of the interface; and $\mathbf{n}$ = unit normal vector. The numerical procedure for enforcing this boundary condition is described now. The value of ζ on the interface is directly calculated with (20) and (21), making use of high-order forward and backward difference equations. Along the interface, tangential second derivatives of ζ are evaluated using centered differences and normal second derivatives of ζ are evaluated by directionally differencing into the porous region. With this information, ψ on the interface can be calculated using (8). Normal velocity on the interface is evaluated according to both open water [(3)] and porous region [(7)] equations, using forward and backward derivatives. From (20) these velocities are set equal to one another, yielding an equation with one unknown, ψ, on the interface, which can now be directly calculated. At this point, all variables have a value along the interface. To maintain the high accuracy of the numerical scheme, all derivatives one grid point from the interface in the normal direction must make use of modified difference equations. Semicentered finite-difference equations must be used, making certain that all terms in the finite difference are in the same region. Application of this interfacial condition has produced accurate results for the 1D problem (Liu and Wen 1997).

For the numerical exterior boundaries, two types of conditions are applied: reflective and radiation. The reflective, or no-flux, boundary condition for the Boussinesq equations has been examined by previous researchers (Wang 1993; Wei and Kirby 1995). This condition is given by

$$\mathbf{n}\cdot\nabla\zeta = \mathbf{n}\cdot\nabla\phi = 0 \tag{22}$$

along the solid boundary. In the porous region, the required condition takes the similar form

$$\mathbf{n}\cdot\nabla\zeta = \mathbf{n}\cdot\nabla\psi = 0 \tag{23}$$

along the solid boundary. The radiation, or open, boundary condition for the Boussinesq equations also have been previously studied (Jiang et al. 1996). This boundary condition allows wave propagation out of the numerical domain and is given

$$\frac{\partial W}{\partial t} \pm c(\mathbf{n}\cdot\nabla W) = 0 \tag{24}$$

along the open boundary, where W represents both ζ and ϕ; c = wave celerity; and the sign depends on the orientation of the open boundary.

The hydraulic conductivity K of the porous breakwater is given (Madsen 1974; Vidal et al. 1988; van Gent 1995)

$$K = \frac{1}{\alpha A + \beta U_c B} \tag{25}$$

where

$$A = \frac{(1-n_e)^3\nu}{gd^2n_e^2}; \quad B = \frac{1-n_e}{gdn_e^3} \tag{26}$$

in which α and β = empirically determined constants; d = characteristic diameter of the porous material; ν = kinematic viscosity of the pore fluid; and U_c = characteristic velocity inside the porous breakwater. The αA term represents the effects of laminar resistance, and $\beta U_c B$ represents turbulent resistance. The characteristic velocity is given (Liu and Wen 1997)

$$U_c = \frac{3}{4}\frac{(u_d^4 - u_u^4)}{(u_d^3 - u_u^3)} \tag{27}$$

where u_d = normal velocity at the downstream face of the breakwater; and u_u = normal velocity at the upstream face of the breakwater. Application of this formula for 1D solitary wave transmission through porous structures has proven to be accurate (Liu and Wen 1997). For the problem with two horizontal dimensions, average normal velocities are found along the upstream and downstream breakwater faces and (27) is again used to find a characteristic velocity.

Uncertainty in evaluating hydraulic conductivity arises from choosing the α and β values. Ideally, one would experimentally determine these values for the specific porous material of interest. This approach, however, eliminates one of the primary benefits of numerical modeling—eliminating or reducing the need to create physical models. Therefore, one would like to be able to take previously determined values of α and β and use them for this analysis. There have been numerous studies that recommend α and β values (Madsen 1974; Vidal et al. 1988; van Gent 1995). The most thorough of these studies was van Gent's work, in which a range of α and β values was experimentally determined, depending on which gravel length scale was used, for a half-dozen different material types. The results of his work indicated that α and β varied widely, depending on what type of porous material was being examined. He concluded, however, that for irregular gravel the average values of α = 1,000 and β = 1.1 were sufficiently accurate to be used over a range of gravel diameters. These values were slightly different from the values of α = 1,100 and β = 0.81 recommended by Vidal et al. (1988) for gravel. A comparison with 1D experimental results is performed to estimate the effect of changing these α and β values.

TRANSMISSION AND REFLECTION OF SOLITARY WAVES

Previously, Liu and Wen (1997) created a 1D model using a similar set of model equations and a completely different numerical scheme. A comparison of experimental maximum transmitted wave heights from Vidal et al. (1988) yielded excellent agreement. However, reflected wave heights and waveform were not compared. To compare them here, additional experimental data are required. A new set of experimental trials were run in the DeFrees Hydraulics Laboratory at Cornell University, Ithaca, N.Y. This wave tank is 30-m long and 1-m wide, with a piston-type wavemaker, the movement of which is controlled by computer. The porous breakwaters were composed of an outer 1.5-cm wire mesh filled with gravel. Two sizes of irregular gravel were used, with median diameters d of 1.6 and 2.0 cm. The measured porosities n_e for both gravel sizes was 0.50. Two breakwater widths b were tested, 15 and 30 cm, and the water depth h was constant for all trials at 10 cm. Solitary waves with amplitudes a of 1–4 cm were generated, and free-surface time series were taken 1 m in front of and 1-m behind the breakwater. All trials were repeated at least once.

The 1D physical system was modeled numerically by specifying a solitary wave as the initial condition. The solitary wave profile and the corresponding potential function are taken (Wang 1993)

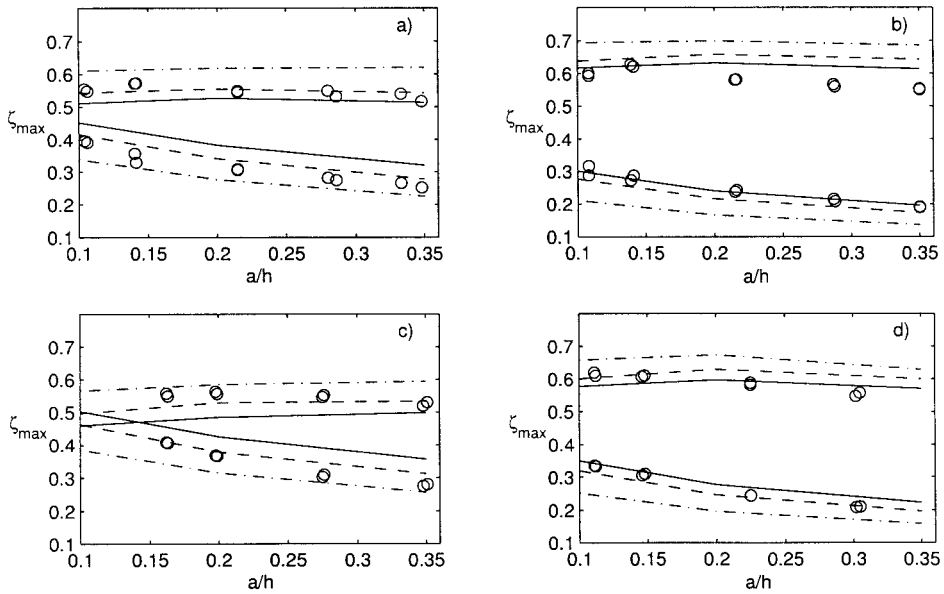

FIG. 1. Transmission and Reflection of Solitary Waves by 1D Porous Breakwater (Transmission Lines Initially Slope Downward: ——, Numerical Results with α = 1,100, β = 0.55; — —, Numerical Results with α = 1,100, β = 0.81; · —, Numerical Results with α = 1,800, β = 1.1; Symbols Represent Experimental Data for *d* = 1.6 cm, *b* = 15 cm; *d* = 1.6 cm, *b* = 30 cm; *d* = 2.0 cm, *b* = 15 cm; *d* = 2.0 cm, *b* = 30 cm)

$$\zeta = \frac{a}{1 + \frac{a}{h}}\left[\text{sech}^2 k(x - ct - x_o) + \frac{a}{h}\,\text{sech}^4 k(x - ct - x_o)\right] \quad (28)$$

$$\phi = h\sqrt{\frac{4}{3}ga}\,[\tanh k(x - ct - x_o) - 1] \quad (29)$$

where

$$k = \frac{1}{h}\sqrt{\frac{3\frac{a}{h}}{4\left(1 + \frac{a}{h}\right)}} \quad (30)$$

$$c = \sqrt{g(h + a)} \quad (31)$$

and x_o = initial location of the solitary wave crest. To compare with the experimental results, numerical simulations for each of the four experimental setups (*d* = 1.6 cm, *b* = 15 cm; *d* = 1.6 cm, *b* = 30 cm; *d* = 2.0 cm, *b* = 15 cm; and *d* = 2.0 cm, *b* = 30 cm) were run. For each setup, three sets of α and β values (α = 1,100, β = 0.55; α = 1,100, β = 0.81; and α = 1,800, β = 1.1) were tried for each solitary wave height, *a*/*h*. Fig. 1 summarizes the experimental and numerical results. Note that the maximum amplitude of the reflected and transmitted waves is scaled by the incident wave height. On average over the four setups, α = 1,100 and β = 0.81 yield the best agreement, with transmitted wave height tending toward a higher degree of correlation than reflected wave height. From examination of Figs. 1(a–d), which are the same gravel size but different breakwater width, one might conclude that the best choice of α and β is weakly dependent on the width of the breakwater. This indicates that the formulation for the hydraulic conductivity of the breakwater is slightly oversimplified. However, with the choice of α = 1,100 and β = 0.81 for both sizes of rock, transmitted wave height can be predicted to within 5% of the incident wave height.

Prediction of the wave heights is an essential measure of the model accuracy, but waveform and phase are equally important, especially for 2D problems when wave-wave interactions become important. To check waveform and arrival time, a free-surface time-series comparison with experimental data is performed. One such comparison is shown in Fig. 2.

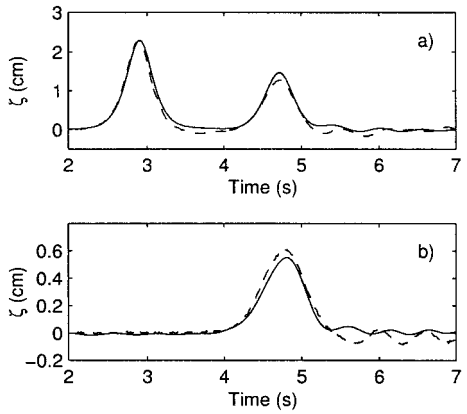

FIG. 2. Comparison between Numerical (——) and Experimental (— —) Time Series for *a*/*h* = 0.225, *b* = 30 cm, *d* = 2.0 cm, α = 1,100, β = 0.81: (a) in Front of Breakwater; (b) behind Breakwater

The arrival time of both reflected and transmitted waves is predicted very well. The arrival time and amplitude of the secondary, trailing waves is not predicted well. In general, the agreement in waveform and arrival time decreases with increasing amplitude, probably due to the weakly nonlinear assumption of the theoretical model.

DIFFRACTION OF SOLITARY WAVES

To date, there are no published experimental data sets for wave interaction with a porous breakwater gap. To validate the model in 2D, a comprehensive set of experiments were performed at Universidad de Cantabria, Santander, Spain. The trials were performed in a 27-m-long, 7-m-wide channel, using an additional 2-m-wide side channel to control the generated waves. A 4-m-long and 0.5-m-wide vertical porous breakwater was located normal to wave incidence, approximately at the center of the channel. Fig. 3 is a plan view of the experimental setup. The porous structure was composed of irregular gravel contained in two steel gabions. A slope of 1/30 exists between the piston-type wavemaker and the breakwater. Leeward of the structure, the solitary waves break on a gravel beach with a 1/13 slope. Water depth, wave height, and gravel diameter were varied to yield a total of eight different trials. Table 1

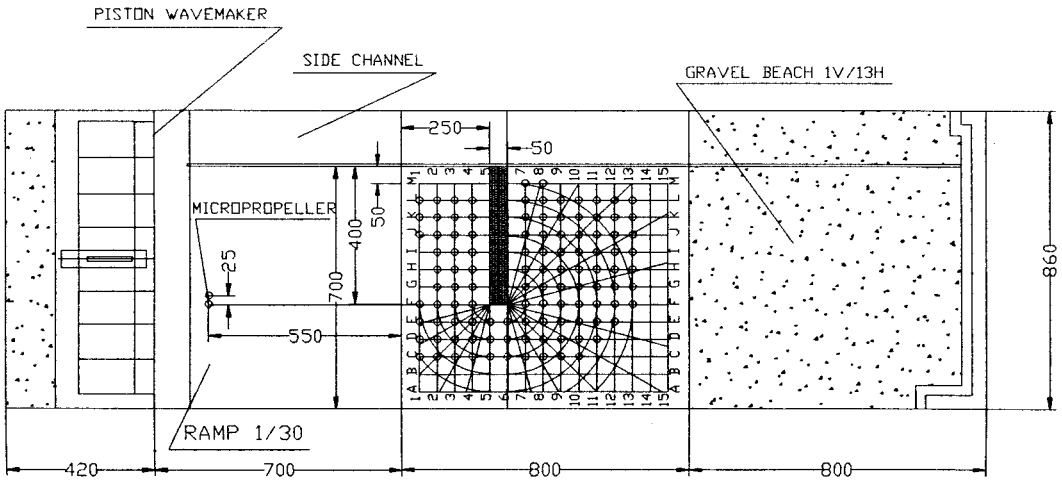

FIG. 3. Plan View of Experimental Setup (Solid Block Represents Porous Breakwater, Small Dots Are Locations Where Free Surface Displacement Time Series Were Recorded)

TABLE 1. Experimental Parameters

Trial (1)	Depth (cm) (2)	Wave height (cm) (3)	d (cm) (4)
1	20	4.2	3.87
2	20	9.3	3.87
3	22	4.2	5.35
4	22	9.2	5.35
5	31	4.0	5.35
6	31	8.8	5.35
7	40	3.8	5.35
8	40	8.3	5.35

summarizes the main characteristics of the cases considered. For each of the trials, free surface elevation was recorded at 110 locations, using a group of 14 gauges with several repetitions. Note that data from Trials 2 and 4 were not used for this analysis because a/h for these trials is near 0.45 and well out of the range of applicability of the weakly nonlinear numerical model.

To numerically model the experimental setup, a solitary wave was sent into the domain through the left boundary, where the wavemaker was located. The wave then traveled up a slope toward the breakwater, just as in the experiments. The side walls were modeled with reflective boundary conditions. The right boundary, leeward of the breakwater, is modeled as an open boundary, allowing the transformed solitary wave to exit the numerical domain.

Although numerical-experimental comparisons were performed for each of the gauge locations for all of the trials, only four of these time-series comparisons are presented in this paper. The comparisons are shown in Fig. 4; the numerical result is the solid line, and experimental data are shown as the dashed line. The location of each comparison is indicated by the lower subplot.

Fig. 4(a) is a comparison in front of the breakwater. The incident and reflected waves are clearly separated. This particular comparison is one of the worst, in terms of wave height, of this trial. The comparison given in Fig. 4(c) is located behind the breakwater, but not in the shadow zone, and shows excellent agreement. Figs. 4(b and d), both located in the shadow zone, also show excellent agreement in both waveform and phase.

To condense all the time-series comparisons for a given trial into one plot, a specific aspect of the comparison must be examined. Maximum wave height, defined as the maximum recorded free-surface elevation at each location, is usually the most important design consideration and, therefore, will be used. The difference in nondimensional maximum wave height between experiment and numerics is inspected. Specifically, this is calculated by

$$\frac{\text{maximum experimental wave height}}{\text{incident wave height}} - \frac{\text{maximum numerical wave height}}{\text{incident wave height}} \tag{32}$$

At each measurement location, for each trial, the above difference is calculated. To get an average difference for all six trials, the absolute value of the difference at each location is taken and then averaged together. Results of the averaging are given in Fig. 5. The black box in Fig. 5 indicates the location of the porous breakwater, and the surrounding gray box shows the inner limits of gauge locations. From this contour plot, it is evident that the numerical model is excellent at predicting wave height. This is especially true in the shadow zone, where the average difference in maximum wave height between the numerical model and experimental trials ranges from 0 to 3% of the incident wave height. This contour plot shows that the numerical model predicts maximum wave height, on average, to within 5% of the incident wave height. The plot also shows that the highest average differences occur near the corners of the breakwater. At these locations, vorticity effects may be important. The numerical model is irrotational, and this lack of numerical vorticity may explain the wave height difference between the numerical model and experiment near the corners. Additional numerical-experimental comparisons, including comparisons for the individual trials, are available via the Internet from ⟨http://www.cee.cornell.edu/porousbwasce/⟩.

The numerical model can accommodate any size domain, limited only by computation resources, with any direction of incident wave. Fig. 6 shows three snapshots of a normally incident solitary wave passing through a porous breakwater gap. This simulation has an incident wave height-to-depth ratio, a/h, of 0.2, the breakwater is 5-water-depths wide and 40-depths long. All of the outer boundaries are reflective boundaries. Fig. 6(a) is the initial condition, with the solitary wave approaching the breakwater from the left. In Fig. 6(b), the transmitted wavefront is nearly aligned with the undisturbed wavefront, and both the reflected wave and the undisturbed wave begin to diffract. The last graphic, Fig. 6(c), shows diffraction patterns both in front of and behind the porous breakwater.

Oblique incidence also can be accommodated. Fig. 7 shows graphs of a 20° obliquely incident solitary wave passing through a porous breakwater gap. The numerical parameters

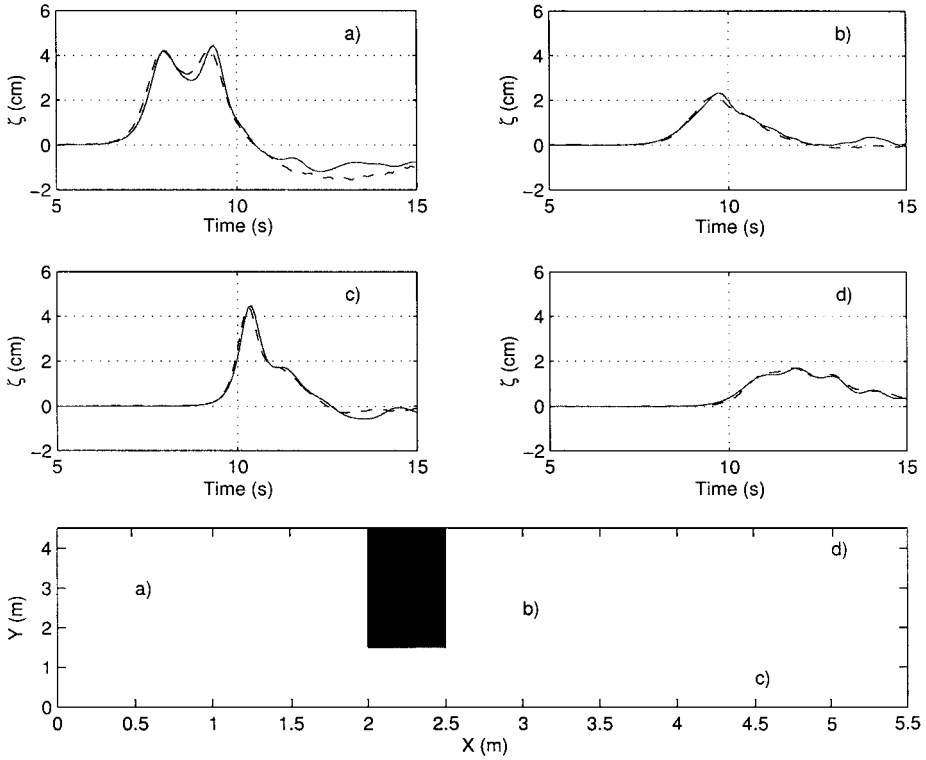

FIG. 4. Comparison between Experimental (— —) and Numerical (——) Runs for Various Locations in Trial 1, with α = 1,100, β = 0.81 (Bottom Subplot Indicates Locations of Time-Series Comparisons, Where Solid Block Is Porous Breakwater and Wave Approaches from Left)

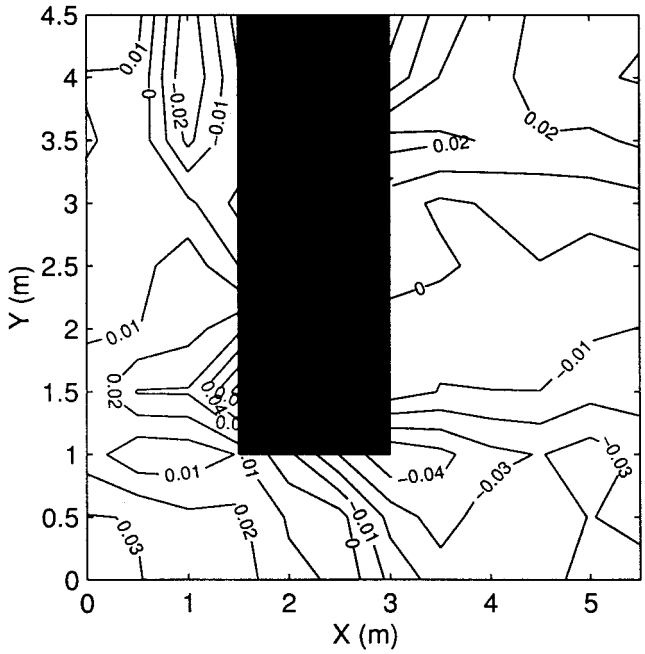

FIG. 5. Absolute Difference in Maximum Wave Height, Normalized by Incident Wave Height, Averaged over All Six Trials

of this case are identical to the normal incidence case except, of course, for the angle of incidence. Open boundary conditions are applied on the right and top boundaries. The initial condition is shown in Fig. 7(a), and in Fig. 7(c) the wave has partially reflected off the front breakwater face. The transmitted wave height for the oblique incident case is about 8% less than the normal incidence case. This is due to the fact that the obliquely incident wave ''feels'' a 6% thicker breakwater.

In the shadow zone of the porous breakwater, wave diffraction is the energy transformation mechanism. However, wave diffraction occurs in two ways. Some of the wave energy diffracts into the calm water behind the transmitted wave, creating a wave with a circular crest line. This form of diffraction is the same as diffraction behind a solid breakwater. Second, wave energy diffracts into the transmitted wavefront from the incident wavefront, due to the discontinuity of wave amplitude. This, the second type of diffraction, is akin to 1D pollutant diffusion, as regions of high and low concentration (wave height) move toward equilibrium. By comparing a solid breakwater with a porous one, one can examine the relative importance of the two types of diffraction.

A solid breakwater is numerically modeled by applying reflective boundary conditions along the solid breakwater faces, where interfacial boundary conditions are enforced for the porous breakwater simulations. To further validate the model, experiments using a solid breakwater were performed at Universidad de Cantabria. The wave basin, measurement locations, and breakwater dimensions were identical to the porous experiments, and water depth and wave heights tested were the same as for Trials 3–8 in Table 1, yielding a total of six different trials. Agreement between the experiments and the model is excellent, with the average difference being <5% at all locations over all six trials of nondimensional maximum wave height (the same percent as in the porous breakwater comparisons). Detailed numerical-experimental comparisons are available via the Internet from ⟨http://www.cee.cornell.edu/porousbwasce/⟩.

Fig. 8 shows six graphics, three of a solitary wave passing a solid detached breakwater (top row) and three of a wave passing a porous detached breakwater (bottom row). In these simulations, the water depth is constant and the scaled wave height, a/h, is 0.1. The breakwaters are 5-water-depths wide and 80-water-depths long. For the porous breakwater, the scaled rock size, d/h = 0.2, n_e = 0.5, α = 1,100, and β = 0.81. In Figs. 8(a and d) the wave height along the front face is at a maximum, and in Figs. 8(b and e) the reflected waves are moving away from the breakwaters and diffraction begins to

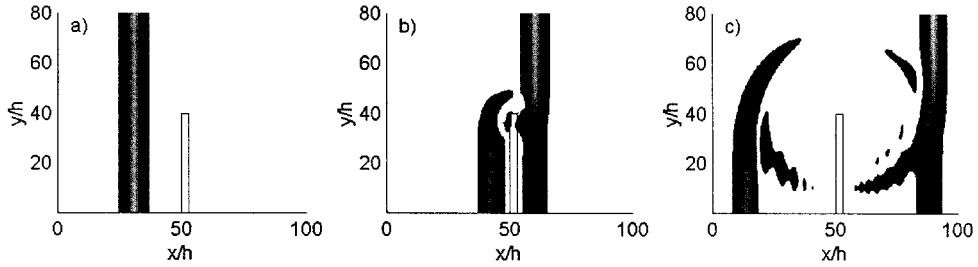

FIG. 6. Spatial Profiles for Normal Incident Solitary Wave Interaction with Porous Breakwater Gap, with a/h = 0.2, b/h = 3, d/h = 0.2, n_e = 0.50, α = 1,100, β = 0.81

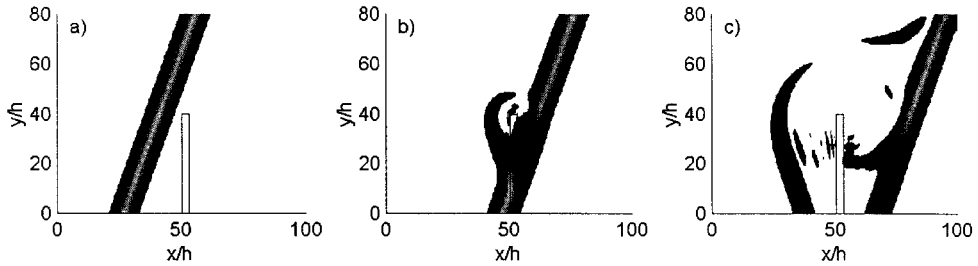

FIG. 7. Spatial Profiles for Oblique Incident (20°) Solitary Wave Interaction with Porous Breakwater Gap, with a/h = 0.2, b/h = 3, d/h = 0.2, n_e = 0.50, α = 1,100, β = 0.81

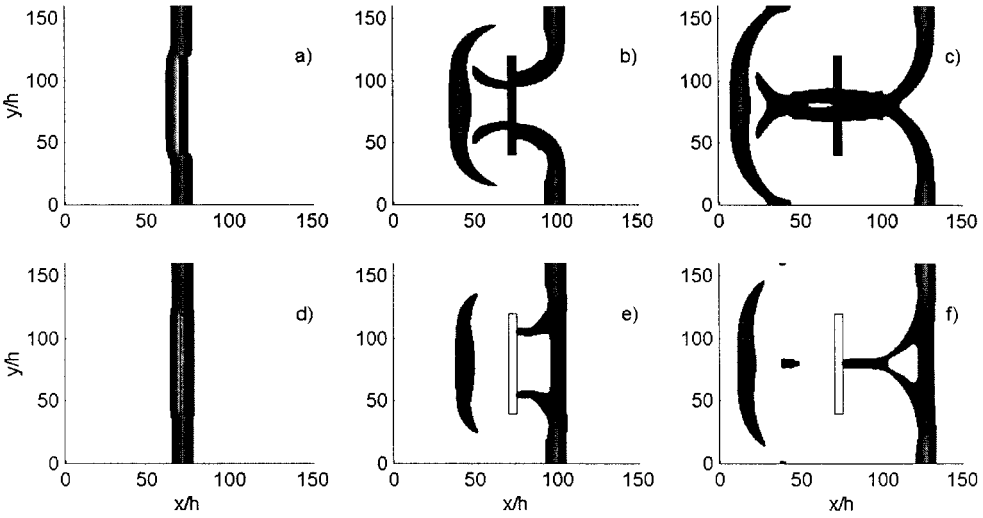

FIG. 8. Spatial Profiles for Normal Incident Solitary Wave Interaction with Solid Detached Breakwater (Top Row) and Porous Detached Breakwater (Bottom Row)

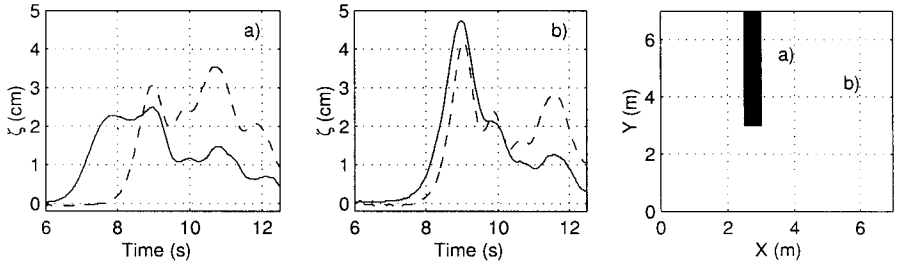

FIG. 9. Experimental Time-Series Comparisons between Solid (— —) and Porous (——) Breakwater for Trial 6 (See Table 1) (Subplot on Right, Where Breakwater Is Shown in Black and Wave Enters from Left, Indicates Spatial Location of Comparisons)

occur behind the breakwater. Examining the shadow zones in Figs. 8(b, c, f, and g), less wave energy is diffracting to form a wave with a circular crest line in the porous breakwater case than in the solid breakwater case. In fact, most of the energy that diffracts in the solid breakwater case to form this circular wave diffracts into the transmitted wavefront in the porous breakwater case. From this example one sees how the relative importance of the two types of diffraction can greatly change the wave field in the shadow zone.

The experimental data also can be used to examine wave field differences between porous and solid breakwaters. Fig. 9 shows two time-series comparisons between a solid and porous breakwater and the corresponding locations. The data are from porous breakwater Trial 6, and the solid breakwater data

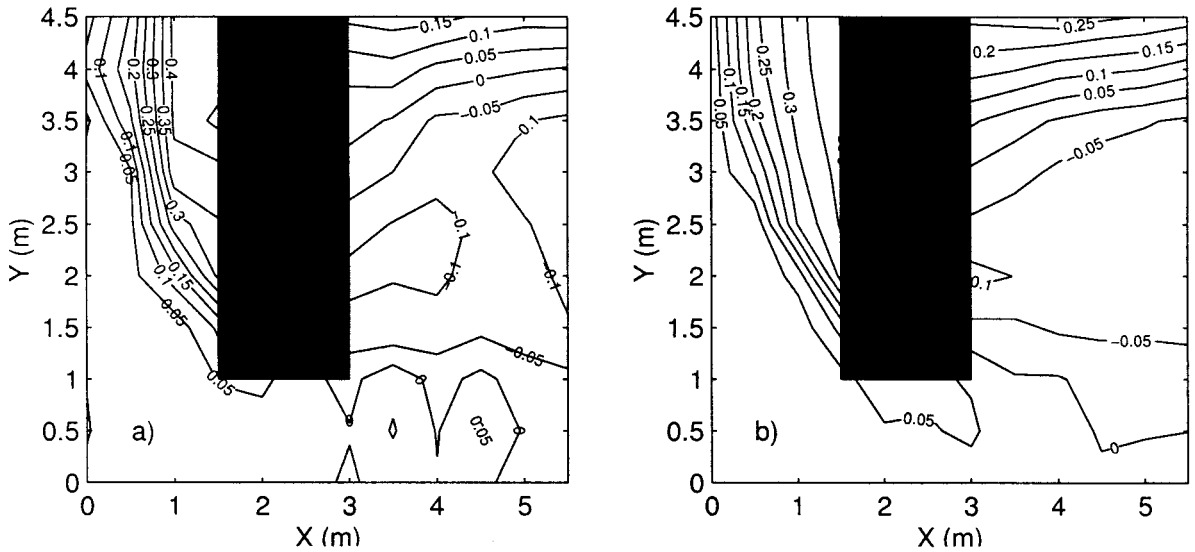

FIG. 10. Difference in Maximum Wave Height, Normalized by Incident Wave Height, between Solid and Porous Breakwater for Trial 3, Using: (a) Experimental Data; (b) Numerical Simulation Results

are from an experiment with the same water depth and wave height as Trial 6. Both comparisons are in the shadow zone, with the comparison in Fig. 9(a) closer to the breakwater than that in Fig. 9(b). In Fig. 9(a), examining the porous breakwater time series, there are clearly two leading maximums, arriving at roughly 8 and 9 s. The first maximum is the transmitted wave, and the second is from the curved diffraction wave. As expected, this curved diffraction wave in the porous breakwater data arrives at the same time as the diffraction wave in the solid breakwater data, as both waves evolve due to the same type of diffraction. The large waves that arrive in both data sets at 11 sec are due to reflection off the channel side wall. Ignoring these reflected waves, one can see that the porous breakwater reduces the maximum wave height at this location by about 20%. At certain locations in the shadow zone, the maximum wave height with a porous breakwater is larger than that with a solid breakwater. Fig. 9(b) is the comparison at one such location, where the porous breakwater wave height is 15% larger. The reason the porous height is larger is the diffraction of incident wave energy into the transmitted wavefront (i.e., the diffraction due to the amplitude discontinuity between the incident and transmitted waves). The waves that arrive at 11.5 s are due to reflection off the channel side wall.

Fig. 9 gives a comparison of wave height at only two locations. It would be useful to see the difference in maximum wave height between solid and porous breakwaters at locations all around the breakwater. Fig. 10 shows the difference in maximum wave height, scaled by incident wave height, between porous and solid breakwaters. The contour plot in Fig. 10(a) is created using experimental data, and the plot in Fig. 10(b) is created using the numerical results. The comparison is from Trial 3, with the solid breakwater trial having identical water depth and incident wave height. At each location the porous breakwater height is subtracted from the solid breakwater height, so positive contours indicate that the maximum wave height is larger with a solid breakwater. As expected, wave height in front of the breakwater is always larger with a solid breakwater. Looking to the shadow zone, there is a swath where the wave height with a porous breakwater is larger, as indicated by the negative contours. Fig. 9(b) is located in this region, and the reasons for the larger height are described above. At all other locations, the wave height with a solid breakwater is larger. Agreement between the experimental [Fig. 10(a)] and numerical [Fig. 10(b)] contour plots is excellent.

CONCLUDING REMARKS

A high-order numerical model, including weak nonlinear and dispersive effects, has been developed for wave interaction with porous structures in the horizontal plane. For both 1D and 2D problems, the model predicts wave height, waveform, and arrival time excellently. The numerical model is validated, on average, to <5% of the incident wave height for breakwaters made of irregular rock. Additionally, the model has been validated for the solid breakwater case. A numerical comparison of solid and porous breakwaters shows how greatly the wave field in the shadow zone differs due to the different diffraction mechanisms occurring. Although only solitary waves have been used in the present analysis, the model could be applied to oscillatory waves. However, the empirical coefficients, α and β, and the formulation for the hydraulic conductivity of the breakwater K might need to be reexamined.

ACKNOWLEDGMENTS

This research was supported in part by a National Science Foundation grant to Cornell University (CTS-9808542) and by the Comision Interministerial de Ciencia y Tecnologia to Universidad de Cantabria under research grant No. MAR96-1833.

APPENDIX. REFERENCES

Coastal Engineering Research Center (CERC). (1984). *Shore protection manual*, U.S. Army Corps of Engineers, Washington, D.C.

Dalrymple, R. A., and Martin, P. A. (1990). ''Wave diffraction through offshore breakwaters.'' *J. Wtrwy., Port, Coast., and Oc. Engrg.*, ASCE, 116(6), 721–741.

Goda, Y., Takayama, T., and Suzuki, Y. (1978). ''Diffraction diagrams for directional random waves.'' *Proc., 16th Int. Conf. Coast. Engrg.*, ASCE, New York, 628–650.

Jiang, L., Ren, X., Wang, K.-H., and Jin, K.-R. (1996). ''Generalized Boussinesq model for periodic non-linear shallow-water waves.'' *Oc. Engrg.*, 23, 309–323.

Liu, P. L.-F. (1984). ''Diffraction of solitary waves.'' *J. Wtrwy. Port, Coast., and Oc. Engrg.*, ASCE, 110(2), 201–214.

Liu, P. L.-F., Lin, P., Chang, K.-A., and Sakakiyama, T. (1999). ''Numerical modeling of wave interaction with porous structures.'' *J. Wtrwy., Port, Coast., and Oc. Engrg.*, ASCE, 125(6), 322–330.

Liu, P. L.-F., and Wen, J. (1997). ''Nonlinear diffusive surface waves in porous media.'' *J. Fluid Mech.*, Cambridge, U.K., 347, 119–139.

McIver, P. (1999). ''Water wave diffraction by thin porous breakwaters.'' *J. Wtrwy., Port, Coast., and Oc. Engrg.*, ASCE, 125(2), 66–70.

Madsen, O. S. (1974). ''Wave transmission through porous structures.'' *J. Wtrwy., Harb. and Coast. Engrg. Div.*, ASCE, 100(3), 169–188.

Madsen, O. S., and White, S. M. (1975). ''Reflection and transmission

characteristics of porous rubble mound breakwaters.'' *Rep. No. 207*, R. M. Parsons Lab., Massachusetts Institute of Technology, Cambridge, Mass.
Penny, W. G., and Price, A. T. (1952). ''The diffraction theory of sea waves by breakwaters, and the shelter afforded by breakwaters.'' *Philosophical Trans. Royal Soc.*, London, Ser. A, 244, 236–253.
Press, W. H., Flannery, B. P., and Teukolsky, S. A. (1989). *Numerical recipes*, Cambridge University Press, Cambridge, U.K., 569–572.
Sollitt, C. K., and Cross, R. H. (1972). ''Wave transmission through permeable breakwaters.'' *Proc., 13rd Int. Conf. Coast. Engrg.*, ASCE, New York, 1827–1846.
Sulisz, W. (1985). ''Wave reflection and transmission at permeable breakwaters of arbitrary cross-section.'' *Coast. Engrg.*, 9, 371–386.
van Gent, M. R. A. (1995). ''Wave interaction with permeable coastal structures.'' PhD thesis, Delft University, Delft, The Netherlands.
Vidal, C., Losada, M. A., Medina, R., and Rubio, J. (1988). ''Solitary wave transmission through porous breakwaters.''*Proc., 21st Int. Conf. Coast. Engrg.*, ASCE, New York, 1073–1083.
Wang, K.-H. (1993). ''Diffraction of solitary waves by breakwaters.'' *J. Wtrwy., Port, Coast., and Oc. Engrg.*, ASCE, 119(1), 49–69.
Wei, G., and Kirby, J. T. (1995). ''A time-dependent numerical code for extended Boussinesq equations.'' *J. Wtrwy., Port, Coast., and Oc. Engrg.*, ASCE, 121(5), 251–261.
Wu, T. Y. (1981). ''Long waves in ocean and coastal waters.'' *J. Engrg. Mech. Div.*, ASCE, 107(3), 501–522.
Yu, X. (1995). ''Diffraction of water waves by porous breakwaters.'' *J. Wtrwy., Port, Coast., and Oc. Engrg.*, ASCE, 121(6), 275–282.
Yu, X., and Togashi, H. (1996). ''Combined diffraction and transmission of water waves around a porous breakwater gap.'' *Proc., 25th Int. Conf. Coast. Engrg.*, ASCE, New York, 2063–2076.